Published in final edited form as:
Sci Signal. ; 7(325): ra44. doi:10.1126/scisignal.2005261.

A Nanoparticle-Based Combination Chemotherapy Delivery System for Enhanced Tumor Killing by Dynamic Rewiring of Signaling Pathways

Stephen W. Morton[1,2,*], **Michael J. Lee**[1,3,*], **Zhou J. Deng**[1], **Erik C. Dreaden**[1], **Elise Siouve**[1], **Kevin E. Shopsowitz**[1], **Nisarg J. Shah**[1], **Michael B. Yaffe**[1,3,4,†], and **Paula T. Hammond**[1,2,5,†]

[1]Koch Institute for Integrative Cancer Research, Massachusetts Institute of Technology (MIT), Cambridge, MA 02139, USA

[2]Department of Chemical Engineering, MIT, Cambridge, MA 02139, USA

[3]Department of Biology and Biological Engineering, MIT, Cambridge, MA 02139, USA

[4]Division of Acute Care Surgery, Trauma, and Critical Care, Department of Surgery, Beth Israel Deaconess Medical Center, Harvard Medical School, Boston, MA 02215, USA

[5]Institute for Soldier Nanotechnologies, MIT, Cambridge, MA 02139, USA

Abstract

Exposure to the EGFR (epidermal growth factor receptor) inhibitor erlotinib promotes the dynamic rewiring of apoptotic pathways, which sensitizes cells within a specific period to subsequent exposure to the DNA-damaging agent doxorubicin. A critical challenge for translating this therapeutic network rewiring into clinical practice is the design of optimal drug delivery

†Corresponding author. myaffe@mit.edu (M.B.Y.); hammond@mit.edu (P.T.H.).
*These authors contributed equally to this work.

SUPPLEMENTARY MATERIALS

www.sciencesignaling.org/cgi/content/full/7/325/ra44/DC1

Fig. S1. Release of doxorubicin visualized by confocal microscopy.
Fig. S2. Biodistribution of Cy5.5-labeled empty liposomes (lacking drug) intravenously administered to mice bearing BT-20 or A549 xenografts.
Fig. S3. Tumor growth monitored by bioluminescence of the firefly luciferase.
Fig. S4. BT-20 tumor bioluminescence in untreated mice, mice treated with single-drug liposomes, or mice treated with dual-drug liposomes.
Fig. S5. A549 tumor bioluminescence in untreated mice, mice treated with single-drug liposomes, or mice treated with dual-drug liposomes.
Fig. S6. Effect of a coadministration paradigm on A549 xenograft growth.
Fig. S7. Effect of pH on the in vitro release of drugs from liposomes containing different combinations of RTK inhibitor and doxorubicin.
Fig. S8. Abundance of cleaved caspase-8, pERK, and γH2AX in A549 or BT-20 cells exposed to different dual drug–loaded folate-functionalized liposomes.
Table S1. Characterization of nonfunctionalized (without folate-PEG) dual drug–loaded and single drug–loaded liposomes.

Author contributions: All authors contributed to the writing and preparation of the manuscript. S.W.M., M.J.L., M.B.Y., and P.T.H. designed all experiments. S.W.M., M.J.L., Z.J.D., E.C.D., E.S., M.B.Y., and P.T.H. contributed to the design, fabrication, and characterization in vitro. S.W.M., M.J.L., Z.J.D., E.C.D., N.J.S., M.B.Y., and P.T.H. contributed to the in vivo characterization presented.

Competing interests: M.B.Y. is a member of the scientific advisory board and stockholder in Merrimack Pharmaceuticals. M.B.Y. and M.J.L. have submitted a patent on the use of temporally staggered therapies involving EGFR inhibitors and cytotoxic chemotherapy agents.

Data and materials availability: Data are available upon request.

systems. We report the generation of a nanoparticle delivery vehicle that contained more than one therapeutic agent and produced a controlled sequence of drug release. Liposomes, representing the first clinically approved nanomedicine systems, are well-characterized, simple, and versatile platforms for the manufacture of functional and tunable drug carriers. Using the hydrophobic and hydrophilic compartments of liposomes, we effectively incorporated both hydrophobic (erlotinib) and hydrophilic (doxorubicin) small molecules, through which we achieved the desired time sequence of drug release. We also coated the liposomes with folate to facilitate targeting to cancer cells. When compared to the time-staggered application of individual drugs, staggered release from tumor-targeted single liposomal particles enhanced dynamic rewiring of apoptotic signaling pathways, resulting in improved tumor cell killing in culture and tumor shrinkage in animal models.

INTRODUCTION

Cancers represent the end states of accumulated genetic transformations that disrupt normal cell signaling events, including those involved in DNA repair, cell cycle regulation, and cell death by apoptosis (1, 2), enabling these mutant cells to proliferate and metastasize. Paradoxically, although defects in DNA damage signaling and response underlie tumor development, they also provide a mechanism for therapeutic tumor cell killing by conventional anticancer cytotoxic therapies, such as chemotherapy or radiation therapy. Undesired effects of these DNA-damaging treatments include the development of highly resistant residual tumors and toxicity to proliferative nontumor tissues, such as the bone marrow and epithelial lining of the gastrointestinal tract. Therefore, there is an important clinical need to identify potent therapeutic strategies that target multiple tumor cell–specific survival pathways to enhance the extent of tumor cell killing and potentially reduce total drug exposure during treatment. Most drug screening efforts have focused on careful selection of drug cocktails based on the underlying biology of the tumor or the response to individual agents. Unfortunately, much less is known about the positive and negative drug-drug interactions for many combination therapies, and the influence of relative dose, dose duration, or timing of delivery has been much less frequently explored (1, 2).

Our recent work validated the impact of timing of drug delivery on the efficacy of multiagent chemotherapy: A pair of drugs that are not particularly beneficial as singular therapies are effective if used in combination when a specific time lag between the administration of each drug is used (3–6). Thus, systematic study of the adaptive responses of signaling networks in tumor cells after an initial drug exposure could be used to design highly effective drug combinations (3).

We recently demonstrated that triple-negative breast cancer (TNBC) cells and non–small cell lung cancer (NSCLC) cells are markedly sensitized to the effects of DNA-damaging chemotherapy by prolonged, but not acute, suppression of epidermal growth factor receptor (EGFR) signaling (3). This sensitization effect resulted from the rewiring of signaling networks upon persistent EGFR inhibition, which unmasked a caspase-8– dependent cell death pathway critical to the ability of doxorubicin and other genotoxins to more effectively kill tumor cells in culture (3). This work demonstrated the importance of drug order and

timing for maximizing the synergistic effects of combination chemotherapy for cancer. However, translating these new findings into the clinic with existing delivery methods is likely to prove challenging because of patient-specific differences in pharmacokinetics, the differing pharmacodynamic parameters for each drug, and the difficulties in targeting both drugs to the same tumor cells in the proper temporal sequence.

To overcome these challenges, we created a robust nanoparticle-based delivery platform capable of producing a precise time-staggered drug release in vivo. Nanoparticles are colloidal material systems commonly composed of organic (such as lipids or polymers) or inorganic (such as silica, iron, or gold) materials and are generally 200 nm or less in size. These structures are commonly used as vectors for controlled drug delivery by containing and protecting the therapeutics from metabolism or destruction. Using this approach, we designed a single nanoparticle construct to serve as a dual hydrophobic-hydrophilic depot for timed sequence of both an EGFR inhibitor and a DNA-damaging agent. This technology facilitated delivery into mice, achieving intracellular colocalization of both drugs and time-sequenced delivery of the synergistic drug combinations. Such an approach, if successful in patients, should mitigate off-target side effects and increase the bioavailability of the drugs, thereby expanding the therapeutic efficacy of selected chemotherapy combinations identified by ongoing systems pharmacology and signaling-based studies.

RESULTS

Dual-drug nanoparticle fabrication

As is typical of most EGFR inhibitors (log *P* ~2 to 6), the EGFR inhibitor erlotinib is highly hydrophobic (log *P* = 2.7), whereas, as is typical of most DNA-damaging agents (log *P* ~1.5 to −1.5), doxorubicin is relatively hydrophilic (log *P* = 0.9). Therefore, this particular drug combination presents a challenge in achieving high concentrations of both drugs in a single nanoparticle. Liposomes, however, provide a unique opportunity to achieve this capability by virtue of their vesicular structure (7, 8). By using the lipid envelope for storage of the hydrophobic drug and the aqueous interior to house the hydrophilic drug, liposomes enable incorporation of high concentrations of both therapeutics and the potential to present them in a shell first, core second fashion to produce the desired sequential staggered release (3)—release of the hydrophobic small-molecule EGFR inhibitor erlotinib from the shell of the nanoparticle before unloading of the cytotoxic doxorubicin from the core.

We fabricated liposomes containing doxorubicin and erlotinib using a lipid film hydration method (9) (Fig. 1A). Lipid vesicles were formed after hydration in an acidic citric acid buffer under high heat and sonication in the presence of the hydrophobic inhibitor erlotinib. Subsequent pH-driven loading of doxorubicin in the interior of the vesicles resulted in the final dual-drug liposomal system (see Materials and Methods) (Fig. 1B). Dynamic light scattering showed that the liposomes prepared in this two-step drug loading process were of uniform size on the basis of their polydispersity index (PDI) (Table 1). We prepared both single-drug (D, doxorubicin) and dual-drug [doxorubicin + erlotinib (DE)] liposomes containing a mixture of lipids in a 56:39:5 mass ratio of DSPC (distearoylphosphatidylcholine)/cholesterol/POPG [1-palmitoyl-2-oleoyl-*sn*-glycero-3-phospho-(1′-*rac*-glycerol)] with *z*-average hydrodynamic sizes (physical size of the

nanoparticle in suspension) relevant for systemic administration and with a ζ potential, measure of surface charge, of −29 mV, indicative of a negatively charged phospholipid exterior. The drugs effectively accumulated in these, yielding a 2.5:1 mass ratio of doxorubicin/erlotinib within the liposomes, from an equal mass supply (3 mg of each drug per 50 mg of lipid used) during fabrication, and the encapsulation efficiency was higher for doxorubicin than for erlotinib (Table 1).

Dual-drug nanoparticle release properties and cytotoxicity in culture

From the compartmentalization of drug in the liposome, we predicted that erlotinib, which is sequestered in the exterior lipid bilayer membrane compartment, would be released before doxorubicin, which is concentrated in the hydrophilic core of the liposomes. To determine the relative release rates of these two drugs, we measured the amount of drug remaining in the liposomes at serial time points after incubation in phosphate-buffered saline (PBS) at physiological pH (7.4) and temperature (37°C). After 24 hours, 60% of the erlotinib had been released, compared to only 20% of the doxorubicin (Fig. 2A). This differential fractional release suggested that spatial control of therapeutic loading into liposomes could enable presentation of this drug combination in the desired fashion for synergistic killing, particularly because the effective local concentration of erlotinib necessary for EGFR inhibition (~100 nM) is much lower than that required for doxorubicin-induced cytotoxicity (2 to 10 μM) (10, 11).

To determine whether the differential release rates from the liposome recapitulated the synergistic cell killing observed previously (3), we applied the dual-drug and single-drug liposomes to BT-20 TNBC and A549 NSCLC cell lines. We observed an increase in apoptosis, monitored by the number of cells positive for cleaved caspase-3 and cleaved poly(adenosine diphosphate–ribose) polymerase (PARP), in response to either liposome, but DE liposomes were more effective at both 24 and 48 hours compared to the single-drug D liposomes (Fig. 2B). The enhanced cleavage of caspase-8, which we have shown previously to occur only in cells treated with time-staggered EGFR-doxorubicin combinations and not in cells co-treated simultaneously with EGFR inhibitors and doxorubicin (3), was detected in both cell lines upon DE liposome treatment (Fig. 2C).

Reduced abundance of phosphorylated extracellular signal–regulated kinase (pERK) occurs in response to EGFR inhibition. We observed reduced pERK abundance in the DE liposome-treated cells, confirming that EGFR activity had been effectively suppressed by release of erlotinib from the dual-loaded nanoparticles (Fig. 2D).

Molecular characterization of liposome-treated cells revealed equivalent amounts of DNA damage, as assessed by γH2AX formation, produced by exposure to either D liposomes or DE liposomes (Fig. 2E). Although both liposomal formulations induced substantial DNA damage (Fig. 2E), the DE formulation produced sustained inhibition of EGFR, as indicated by a reduction in pERK for up to 72 hours (Fig. 2D), and was more cytotoxic, as indicated by the larger apoptotic response (Fig. 2, B and C).

Nanoparticle modifications to improve tumor targeting in vivo

To further improve the utility of this time-staggered drug delivery for in vivo use, we prepared liposomes with folate and polyethylene glycol (PEG) as a means of minimizing protein adsorption and subsequent nonspecific clearance while promoting tumor targeting (12–17). Folate is a commonly used ligand for targeted cancer delivery because it enhances delivery of therapeutics to tumor cells on which folate receptor a is abundant at the cell surface. Of particular interest for this investigation, as many as two of three patients with NSCLC and TNBC, as well as many other cancer cell types including tumors of the ovary and prostate, have tumors with abundant folate receptors (18). Thus, to enhance tumor targeting, we included a folate-functionalized lipid, 1,2-distearoyl-*sn*-glycero-3-phosphoethanolamine–*N*-PEG-5000 (DSPE-PEG_{5K}), with a PEG-5000 linker (DSPE-PEG_{5K}-folate) in the lipid formulation at a 0.5 mole percent (mol %) ratio to the total lipid composition. We also included a shorter PEG-2000 linker lipid (DSPE-PEG_{2K}) at an equivalent 0.5 mol % ratio to minimize protein adsorption and opsonization of the liposomes while still enabling access to the folate group on the longer PEG linker (Fig. 3A). This type of targeted liposomal design has been used to deliver single-drug therapies (12, 13, 15–17, 19).

The resulting single drug–loaded liposomes with doxorubicin, folate, and PEG (DFP) and the dual drug–loaded liposomes with doxorubicin, erlotinib, folate, and PEG (DEFP) were uniform, with a slight reduction in negative ζ potential compared to the uncoated liposomes, because of the addition of PEG to the surface, and a corresponding ~10 to 15% increase in size from the uncoated liposomes (Table 1). Thus, the addition of folate and PEG on the drug-loaded liposomal exterior only resulted in a moderate increase in particle size, which is important for systemic administration to minimize physical filtration of the nanoparticles by the liver and spleen and enhance tumor accumulation.

To demonstrate the cell targeting capabilities of these functionalized liposomes, we labeled doxorubicin-loaded, folate-functionalized liposomes with the near-infrared (near-IR) dye Cy5.5 (DFP-Cy5.5) by including the Cy5.5-labeled PEG-2000–lipid conjugate DSPE-PEG_{2K}-Cy5.5 at 0.1 mol %, which enabled fluorescent tracking (15, 16) in vitro and in vivo. We also created nonfunctionalized PEG liposomes labeled with Cy5.5 (DP-Cy5.5) but lacking the folate (table S1), so that we could determine the effect of folate targeting on the cellular uptake of the liposomes. We analyzed nanoparticle uptake by confocal microscopy (Fig. 3B) and flow cytometry (Fig. 3C) of both BT-20 and A549 cells after 1-hour incubation with Cy5.5-labeled liposomes either containing the folate for cell targeting (DFP-Cy5.5) or lacking the folate (DP-Cy5.5). After incubation with the targeted liposomes (DFP-Cy5.5), both cell lines exhibited particle fluorescence (red) throughout the cell cytosol, suggesting uptake and endosomal escape of the liposomal contents (Fig. 3B). Analysis by flow cytometry confirmed that both cell lines exhibited enhanced uptake of folate-containing liposomes compared with that of the liposomes without folate (Fig. 3C) and showed that saturation occurred at high concentrations of folate-containing liposomes. The folate-containing liposomes not only resulted in substantially greater uptake of the nanoparticles by the cells but also increased the concentration of doxorubicin associated with each cell line (Fig. 3C). For the untargeted systems, it is likely that most of the doxorubicin that

accumulates in the cells results from nonspecific liposomal uptake or occurs by pinocytosis of the free drug that is released into the media by the liposomes. We compared the uptake and nuclear accumulation of DFP-Cy5.5 liposomes with that of free doxorubicin by confocal microscopy, which confirmed that uptake and nuclear accumulation were delayed when delivered by the nanoparticles (fig. S1).

Effectiveness of dual-drug nanoparticles in reducing tumor burden in mice

To evaluate these systems for tumor remediation in vivo, we first examined the pharmacokinetics of the folate-PEG–functionalized empty nanoparticles (lacking drugs) injected intravenously into healthy BALB/c mice, which are immune-proficient. The folate-PEG–functionalized, Cy5.5-labeled empty liposomes (NFP-Cy5.5) exhibited relatively low liver accumulation as a function of time (14, 23, 17, 14, and 12% injected dose, respectively, based on fluorescence recovery, at 30 min, 9 hours, 24 hours, 48 hours, and 72 hours, respectively) (Fig. 4A). In the circulation, NFP-Cy5.5 exhibited half-lives of 2.2 and 11.1 hours, representing rapid and slow elimination phases calculated on the basis of a two-compartment model (Fig. 4B). Furthermore, visualization of firefly luciferase–expressing tumors revealed NFP-Cy5.5 liposome accumulation in the tumors of xenograft-bearing nude mice up to 30 days after a single injection of the folate-targeted liposomes; we observed 2% injected dose at 9 hours, 5% injected dose at 24 hours, and 7% injected dose after 30 days on the basis of fluorescence recovery (Fig. 4C). We also observed lower intensity liposome fluorescence in other tissues, such as the liver, kidneys, and brain (fig. S2). Thus, the formulated folate-targeted liposomal systems accumulated appreciably in the target tissue (xenograft tumors), as well as the liver, kidneys, and brain, for a prolonged period.

Because tumor size in BT-20 and A549 xenograft models scaled with bioluminescence of the firefly luciferase–expressing tumors measured with the live animal imaging system (fig. S3), we could quantify tumor size in situ during treatment. We compared the effectiveness of the administration of DEFP liposomes or DFP liposomes in limiting or reducing tumor growth in the BT-20 TNBC and A549 NSCLC xenograft models (Fig. 5, A and B, and figs. S4 and S5). Twenty-two days after the tumor cells had been injected and tumors were established (fig. S3), a single administration of the dual drug–loaded (DEFP) liposome (2 mg/kg) produced tumor regression by day 32, whereas the single drug–loaded DFP liposomes and the untreated control mice exhibited continued tumor growth (Fig. 5, A and B). In some of the untreated control mice injected with A549 cells, tumors grew rapidly, reaching the maximum allowed tumor burden (figs. S4 and S5). Significant tumor shrinkage was only observed for combination therapy–treated mice bearing xenografts for each cell line.

We also tested the effectiveness of co-delivery of doxorubicin and erlotinib. Because it was difficult to achieve simultaneous delivery with a single liposomal nanoparticle for this drug combination, we designed single-drug delivery systems for each drug in the combination therapy and administered them together to mimic a co-release behavior. We co-injected DFP (2 mg/kg) with cyclodextrin-erlotinib (hydroxylpropyl-β-cyclodextrin) in PBS at 0.5 mg/kg in A549 xenograft–bearing mice, followed by repeated dosing of cyclodextrin-erlotinib at days 2 and 4 to supply additional erlotinib to match the slow, sustained release of

doxorubicin (fig. S6). Although some inhibition of tumor growth was observed at day 3, later the tumors exhibited increased growth. Thus, simultaneous, sustained co-administration was a less effective treatment, resulting in tumor growth. In contrast, tumor shrinkage and regression was achieved with staged combination therapeutics packaged in the same nanoparticle delivery vehicle.

Expanding the drug combinations incorporated into the dual-drug nanoparticles

Thus far, we extensively characterized a time-staggered doxorubicin/erlotinib combination liposome that effectively and significantly reduced xenografted tumor growth. We examined whether this platform could be adapted for delivery of other therapeutic combinations. We interchanged the cytotoxic drug encapsulated in the aqueous compartment [doxorubicin (D) or cisplatin (C)] and incorporated one of the following [receptor tyrosine kinase (RTK)] inhibitors of signaling by EGFR family members into the lipid envelope: erlotinib (E), gefitinib (G), afatinib (A), or lapatinib (L). The physicochemical properties of the nanoparticles, including size distribution and drug loading efficiency, with the different drug combinations were similar (Tables 2 and 3). In vitro drug release kinetics were similar for each of the combinations, with rapid release of the RTK inhibitor followed by a sustained release of the cytotoxic agent (Fig. 6A and fig. S7). We examined the ability of each drug combination–folate– targeted liposome (DAFP, DEFP, DGFP, DLFP, CAFP, CEFP, CGFP, CLFP) to mediate cell death in culture by analyzing caspase-3 and PARP cleavage in BT-20 and A549 cells (Fig. 6, B and C). Some combinations were more effective at promoting tumor cell death, whereas others had little effect on the absolute magnitude of cell death but accelerated the rate at which the cells died. Compared to the A549 cells, BT-20 cells were typically more sensitive to the cytotoxic effects of any of the single cytotoxic agents or the dual drug–loaded liposomes, exhibiting >80% cell death in most conditions. Within each cell line, there were some differences in cytotoxicity. For example, the afatinib-cisplatin combination was the most effective of the cisplatin-containing combinations in promoting A549 cell death (~20%), whereas ~40 to 50% of these cells were apoptotic when exposed to any of the doxorubicin-containing combinations. For the BT-20 cells, the cisplatin-erlotinib and cisplatin-afatinib combinations produced the fastest apoptotic response, which might be an important determinant of efficacy in vivo; however, the maximum percent of apoptotic BT-20 cells was similar for all dual drug–loaded liposome combinations. The cisplatin combinations were generally no more effective at producing cell death as cisplatin alone, with the exception of the cisplatin-afatinib combination, which produced a higher maximal cell death than any other combination or cisplatin alone in A459 cells.

We also examined the different doxorubicin- and RTK-loaded liposomes for caspase-8 cleavage, as well as their effect on the extent of DNA damage, as indicated by the abundance of γH2AX, and on downstream signaling, as indicated by pERK abundance (fig. S8).

DISCUSSION

Here, we used knowledge of synergistic combination therapies that rewire signaling pathways and networks (3). However, the synergistic therapeutic response exhibits a

pronounced dependence on timing and sequence of drug release. Therefore, we packaged the drugs together in a systemically administrable tumor-targeted drug carrier, a liposome-based nanoparticle. Some success toward implementing synergistic cancer therapies using engineered delivery systems had been achieved previously (7, 8, 20–26). These previous strategies have largely focused on the simultaneous release of drugs from a single delivery platform using various techniques, including covalent linkage of drug to the material comprising the nanoparticle or encapsulation within the nanomaterial. Although these approaches have demonstrated the enhanced therapeutic efficacies of drug combinations, there has been no development to date of time-staggered release platforms that are specifically designed to engage and rewire cancer survival pathways.

We found that differential release rates of the drugs occurred in the correct sequence from a single nanoparticle platform and that the dual drug– loaded liposomes were cytotoxic to cultures of A549 and BT-20 cells. Molecular readouts (caspase-8 cleavage, pERK, γH2AX) further confirmed that the multidrug liposomes disrupted cell function in the expected sequence with early and sustained suppression of EGFR signaling, thereby rendering the cells susceptible to apoptosis in response to later exposure to toxic amounts of DNA-damaging agents. Furthermore, modification of the combination drug–loaded liposomes to include folate and PEG promoted tumor targeting in vivo for enhanced efficacy against A549 and BT-20 xenograft tumor models compared to single-drug treatment alone.

The efficacy of these staggered release nanoparticle systems containing a small-molecule inhibitor with a cytotoxic agent presents a new therapeutic option for cancer therapy. By exploiting the intrinsic two-compartment property of a liposomal system, combination therapeutics with different physiochemical properties (hydrophilic and hydrophobic) were compartmentalized with reasonable efficiencies in a core-shell fashion that facilitated the staggered release observed. Because liposomal systems provide high levels of control over fabrication and modularity (9), this type of nanoparticle systems should enable customizable targeting to specific tumors, as well as loading of therapeutic agents tailored to specific treatment regimens.

The drugs that we tested were naturally hydrophobic (erlotinib, afatinib, gefitinib, and lapatinib) or hydrophilic (doxorubicin and cisplatin), and this nanoparticle system should be adaptable to combinations that have chemically similar properties as these two combinations (RTK inhibitor and cytotoxic agent). However, staggered release that relies on the core versus outer layer loading of the two drugs may not always be attainable. Therefore, other technologies, such as layer-by-layer assembly of polyelectrolytes, can facilitate coatings on the exterior of drug-loaded nanoparticles to incorporate both hydrophilic and hydrophobic molecules (27), to introduce compartmentalization of two or more drugs and enable control over timing and sequence of drug release. Further, conjugation of one therapeutic to the nanoparticle core followed by encapsulation or coating on this core could further promote the staggered release necessary to elicit synergism between drug combinations. Finally, combinations that require delivery to the same cell for optimal synergistic efficacy further demonstrate the importance of encapsulating multidrug combinations within a single nanoparticle formulation.

The complexity of growth, survival, and death signaling pathways in cancers continues to motivate investigation using systems biology approaches to inform treatments against cancer (4, 28). Furthermore, with the growing appreciation that the pathways change in response to treatment or drug exposure, development of delivery systems that are safe, yet capable of sophisticated levels of control over the delivery, timing, or sequence of release, to therapeutically rewire these signaling pathways is essential to translate findings to the clinic. Here, we addressed this challenge by developing a simple delivery platform to target specific cancer cell types that are responsive to sets of synergistic drugs with predetermined staged treatment regimens. Future tuning and adaptation of these systems using nanomaterials design approaches should greatly enrich the range of signaling pathway–based drug combinations and synergistic time-dependent release profiles that can be achieved for targeted tumor therapy through dynamic network rewiring.

MATERIALS AND METHODS

Study design

Erlotinib and doxorubicin as a combination therapeutic treatment have been previously shown to enable synergistic cell death in certain cell types when administration of the therapeutics is manually time-staggered (3). We sought to achieve this temporal control over release in a systemically administrable nanoparticle formulation. For efficacy evaluation of these systems, power analysis was performed with G*Power Analysis, using repeated-measures ANOVA with between-subjects factors. We assumed an effect size of 0.5, an error probability of 0.05, a power of 0.95, and a correlation of 0.2. To achieve statistical significance, we used 15 animals bearing dual rear xenografts—5 in each experimental group. Endpoints were predetermined for evaluation of the biological performance of these systems, as well as for those experiments investigating tumor burden of the animals after treatment. All experiments were randomized and nonblinded.

Materials

All lipid components were purchased from Avanti Polar Lipids, except for cholesterol from Sigma. All therapeutics were purchased from LC Laboratories, except for cisplatin [*cis*-diammineplatinum(II) chloride] from Sigma. All other chemicals (citric acid, sodium citrate, and sodium carbonate) and solvents (chloroform, methanol, and PBS) were purchased from Sigma.

Liposome preparation

Liposomes were formulated at a mass ratio of 56:39:5 (DSPC/cholesterol/POPG). These three components were dissolved, along with the small-molecule inhibitor (weight ratio to total lipid weight, 3:50), in a 2:1 mixture of chloroform/methanol. A thin film of these materials was generated by rotary evaporation at 40°C at 150 mbar. This film was desiccated overnight until completely dry. Hydration of the lipid film was conducted at 65°C under sonication in 300 mM citric acid buffer (pH 4) for 1 hour. The pH of the liposomal suspension was then adjusted to ~6.5 by addition of 300 mM sodium carbonate buffer to create a gradient between the exterior and interior compartments. Functionalization with DSPE-PEG_{5K}-folate and DSPE-PEG_{2K}, with or without DSPE-PEG_{2K}-Cy5.5, was

conducted after fabrication using a post-insertion technique in which micelles (in 0.9% sodium chloride solution) of the components desired to incorporate on the liposomal surface were incubated with the prepared drug-loaded liposomes for 30 min, after which they were filtered through a 0.2-μm PES (polyethersulfone) syringe filter. The cytotoxic drug (doxorubicin, 3 mg; cisplatin, 10 mg) was added in a 0.9% sodium chloride solution (1 ml) to load through a pH gradient method. To facilitate solubilization of the cytotoxic agents, the dispersed solution was sonicated at 65°C for 5 min. The final combination drug–loaded system was subsequently exchanged into PBS (pH 7.4) after centrifugal filtration [100,000 molecular weight cutoff (MWCO); Millipore] to remove the high-salt buffer (citric acid, sodium carbonate) and any unloaded drug. Empty (lacking drug) liposomes (NFP) were formulated using the same procedure.

Liposome characterization

Dynamic light scattering and ζ potential analysis were conducted in 10 mM sodium chloride at 25°C using a Malvern ZS90 zeta-sizer. HPLC (Agilent Technologies) and NanoDrop absorbance measurements (345 nm for inhibitor; 480 nm for doxorubicin) were used to validate drug loading of the inhibitor (λ_{abs} = 345 nm) and doxorubicin (λ_{abs} = 480 nm). Cisplatin concentration was quantified by a colorimetric assay using *o*-phenylenediamine against a standard curve (29). Cryo-transmission electron microscopy was conducted by imaging a vitrified dilute sample of the liposomal suspension at 120 kV and 77 K.

Nanoparticle drug release in vitro

Liposomes were incubated under sink conditions [1-liter sink for 1 ml of liposome suspension] in 1× PBS under agitation in 1 ml of 3500 MWCO Float-A-Lyzer (Spectrum) at 37°C. PBS was replenished each day of the experiment. Samples were taken of the liposomes to quantify remaining drug concentrations by HPLC [after dissolution in a 50:50 mixture of acetonitrile/water (pH 5)] and absorbance measurements (NanoDrop) [345 nm for erlotinib, lapatinib, gefitinib, or afatinib; 480 nm for doxorubicin].

Confocal microscopy

Images were taken with a Nikon A1R Ultra-Fast Spectral Scanning Confocal Microscope (Nikon instruments Inc.). BT-20 and A549 cells were seeded in CELLview glass-bottom dishes (Greiner Bio-One GmbH) at 1×10^5 cells per well and grown overnight in Opti-MEM (Gibco, Life Technologies). For the data displayed in Fig. 2, cells were then incubated with empty (no drug, NP-Cy5.5, NFP-Cy5.5) Cy5.5-labeled liposomes for 1 hour at 37°C. At the end of this period, cells were washed, fixed with paraformaldehyde, permeabilized with Triton X-100, and stained with phalloidin-568 for 30 min, followed by the addition of 4′,6-diamidino-2-phenylindole (DAPI) for an additional 10 min, after which they were washed (with Opti-MEM) and imaged (in Opti-MEM) at the DAPI (excitation, 360 nm; emission, 460 nm) and Cy5.5 channels (excitation, 640 nm; emission, 700 nm). For the data displayed in fig. S8, live cell imaging was performed by exposing A549 cells to DFP-Cy5.5 or free doxorubicin in Opti-MEM and serially imaging the cells at the DAPI (excitation, 360 nm; emission, 460 nm), doxorubicin (excitation, 480 nm; emission, 560 nm), and Cy5.5 (excitation, 640 nm; emission, 700 nm) channels.

Flow cytometry

Measurements were performed using a BD LSR Fortessa-HTS coupled with a high-throughput system for the 96-well plate format (BD Biosciences). Doxorubicin fluorescence was measured after excitation at 488 nm and detected at 530 nm; Cy5.5 fluorescence was measured after excitation at 640 nm and detected at 710 nm. Cell association data were presented as geometric mean fluorescence collected in triplicate after cell incubation with empty and doxorubicin-loaded Cy5.5-labeled liposomes for 1 hour at 37°C.

Apoptosis

Measurements were conducted as previously described (3). Briefly, after the treatment time course, cells were washed, trypsinized, fixed in 4% paraformaldehyde for 15 min at room temperature, resuspended in ice-cold methanol, and incubated overnight at −20°C. Cells were then washed twice in PBS-Tween and stained with antibodies against cleaved caspase-3 and PARP. Secondary Alexa-conjugated antibodies were used for visualization in a BD FACSCalibur flow cytometer.

Western blotting

Experiments were performed as previously described (3). Briefly, cell lysates were prepared in a manner that enabled samples to be used for both Western blot analysis and reversed-phase protein microarray. Cells were washed twice in PBS and lysed directly on the plate in a buffer containing 50 mM tris-HCl, 2% SDS, 5% glycerol, 5 mM EDTA, 1 mM NaF, 10 mM β-glycerophosphate, 1 mM phenylmethylsulfonyl fluoride, 1 mM Na_3VO_4, and phosphatase and protease inhibitors (Roche complete protease inhibitor tablets and PhosSTOP tablets). Crude lysates were filtered using an AcroPrep 96-well 3.0-μm glass fiber/0.2-μm BioInert filter plate (Pall) and normalized for protein content using the bicinchoninic acid protein assay (Pierce). For Western blots, lysates were run on 48-well precast gels and transferred using a semidry fast transfer apparatus onto nitrocellulose membranes (E-PAGE, iBlot, Invitrogen). Blots were blocked in Odyssey Blocking Buffer (Li-COR Biosciences), incubated overnight with primary antibody, stained with secondary antibodies conjugated to an IR dye, and visualized using an Odyssey flat bed scanner (Li-COR Biosciences).

Antibodies against γH2AX, pERK, and cleaved caspase-8 were purchased from Cell Signaling Technology. Antibodies against β-actin were purchased from Sigma. Raw signals for each protein of interest were quantified and background-subtracted using the Li-COR Odyssey software and divided by β-actin signals to normalize for loading differences, and then each normalized signal was divided by a reference sample contained on each gel for gel-to-gel normalization.

Pharmacokinetics

All animal experimentation adhered to the National Institutes of Health (NIH) *Guide for the Care and Use of Laboratory Animals* and was in accordance with institutional guidelines. BALB/c female mice (Taconic) were systemically administered (tail vein) empty Cy5.5-labeled liposomes (NFP-Cy5.5) at a concentration of 3 mg/ml [corresponding radiant

efficiency, measured by the whole-animal imaging system (IVIS, Xenogen, Caliper Instruments) of 0.1-ml sample injected in each mouse, ~1×10^{10}]. Whole-animal fluorescence imaging (IVIS, Xenogen, Caliper Instruments) was performed at the indicated time points for one cohort of mice ($n = 3$), and a separate cohort was used for retro-orbital bleeds to determine the circulation half-life of the system. Imaging and circulation data presented were normalized to autofluorescence (imaged animals, isolated blood) obtained before injection. Results of the analysis of circulation data based on recovered fluorescence normalized to preinjection blood autofluorescence are displayed with a two-compartment model fit (both slow and fast half-lives presented).

Tumor targeting and regression

Tumor targeting data were obtained by imaging a Cy5.5-labeled DSPE-PEG-Cy5.5 lipid that was inserted into the liposomal membrane. This dye-labeled lipid was functionalized using a DSPE-PEG-NH_2 lipid (Nanocs) and Cy5.5-NHS (Lumiprobe) at a 1:1 ratio in dimethyl sulfoxide at 4°C for complete labeling of the lipid. Final dye-labeled lipid product was lyophilized and stored as a powder at −20°C. Tumor-targeting data were collected using a near-IR imager (IVIS, Xenogen, Caliper Instruments) at $\lambda_{ex} = 675$ nm, $\lambda_{em} = 720$ nm. Percent injected dose calculations were performed from fluorescence intensity of the tumors, after background subtraction of preinjection tissue autofluorescence, and normalized to the amount of fluorescent material injected. Luminescent xenograft tumors were seeded after stable transfection of BT-20 and A549 cells with the firefly luciferase plasmid. This enabled assessment of tumor size by a visual and quantifiable luminescent readout generated by whole-animal imaging (Xenogen, Caliper Instruments). Cells were mixed in a 1:1 ratio with BD Matrigel Basement Membrane Matrix to a final density of 5×10^7 cells/0.1 ml injection. The matrix-cell suspension (0.1 ml) was injected in each rear hind flank of NCR nude mice (Taconic). Tumors were allowed to grow until a visible tumor was established, and luminescence monitoring was indicative of solid tumor growth (see fig. S3, ~7×10^8 radiance final luminescent readout from each xenograft). Xenograft-bearing NCR nude mice were then systemically administered therapy (DFP, DEFP) in a 0.1-ml injection at a concentration of 2 mg/kg (based on doxorubicin loading) and monitored for 32 days. Luminescence images were obtained by 0.1-ml intraperitoneal injections of D-luciferin (30 mg/kg; Caliper) and imaging (IVIS, Xenogen, Caliper) with an open luminescence filter 15 min after injection. These data are presented, along with region of interest quantification of radiance corresponding to the xenograft-specific luminescence for each mouse treated. Data are normalized for each mouse against the tumor luminescence before injection and presented as fold luminescence above this measurement. $n = 5$ for each treatment (untreated, DFP, DEFP), and data correspond to mean ± SEM for each treatment group. An unpaired, two-tailed t test comparing the single-drug (DFP) and combination drug (DEFP) systems was performed to determine statistical significance. A control simulating the simultaneous release of both doxorubicin and erlotinib was performed in vivo by the systemic co-administration of DFP liposomes (1 mg/kg) and an erlotinib-cyclodextrin complex (CD-Erl) in PBS (1 mg/kg, hydroxypropyl-β-cyclodextrin) 22 days after xenografts were established. Subsequent booster doses of erlotinib were systemically administered at 1 mg/kg on days 2 and 4. Live animal bioluminescence images of hind-flank A549 xenografts shown before treatment (pre) and at days 3, 10, and 30 were collected. Quantification of luminescence

[radiance (photons)], normalized to preinjection tumor luminescence, is displayed on a semilog plot as average fold change in luminescence ± SD (normalized to preinjection tumor luminescence).

Statistical analyses

Prism 5 (GraphPad) was used for all analyses. Results are presented as mean ± SEM, unless otherwise noted. Efficacy data were analyzed by an unpaired, two-tailed t test and repeated-measures one-way ANOVA comparing all groups to assess significance in treatment. $P < 0.05$ was considered significant.

Supplementary Material

Refer to Web version on PubMed Central for supplementary material.

Acknowledgments

We wish to dedicate this work to the memory of Officer Sean Collier, for his caring dedication to the Massachusetts Institute of Technology (MIT) community and sacrifice. S.W.M. would like to further dedicate this work to his loving father and hero, Kenneth Reid Morton, who passed away December 20, 2013. We would like to thank the Koch Institute for Integrative Cancer Research at MIT for providing resources (facilities, funding) central to the completion of this work, specifically the Koch Institute Swanson Biotechnology Center core facilities (microscopy—E. Vasile, flow cytometry—G. Paradis and M. Jennings, whole-animal imaging—S. Malstrom) for facilitating biological data, as well as the MIT Department of Comparative Medicine for husbandry and general animal care. We would also like to thank B. Aitken and M. A. Quadir for their contribution of valuable resources and input.
Funding: We would like to acknowledge funding for valuable resources to facilitate this work. These include grants from the NIH and Center for Cancer Nanotechnology Excellence, grant nos. P30-CA14051, U54-CA151884, U54-CA112967, R01-ES015339, and R21-ES020466, and a Breast Cancer Alliance Exceptional Project Grant. S.W.M. would like to acknowledge funding from the National Science Foundation Graduate Research Fellowship. Z.J.D. would like to acknowledge the CJ Martin Fellowship from the National Health and Medical Research Council. E.C.D. would like to acknowledge the NIH fellowship: Kirschstein NRSA 1F32EB017614-01. K.E.S. would like to acknowledge the National Sciences and Engineering Research Council for a postdoctoral fellowship. M.B.Y. and P.T.H. acknowledge David H. Koch faculty appointments. This work was also funded through the Koch Institute Frontier Research Program supported by the Kathy and Curt Marble Fund for Cancer Research.

REFERENCES AND NOTES

1. Weinberg, RA. The Biology of Cancer. New York: Garland Science, Taylor & Francis Group LLC; 2007. p. 864
2. Hanahan D, Weinberg RA. Hallmarks of cancer: The next generation. Cell. 2011; 144:646–674. [PubMed: 21376230]
3. Lee MJ, Ye AS, Gardino AK, Heijink AM, Sorger PK, MacBeath G, Yaffe MB. Sequential application of anticancer drugs enhances cell death by rewiring apoptotic signaling networks. Cell. 2012; 149:780–794. [PubMed: 22579283]
4. Fitzgerald JB, Schoeberl B, Nielsen UB, Sorger PK. Systems biology and combination therapy in the quest for clinical efficacy. Nat. Chem. Biol. 2006; 2:458–466. [PubMed: 16921358]
5. Kong DX, Li XJ, Zhang HY. Where is the hope for drug discovery? Let history tell the future. Drug Discov. Today. 2009; 14:115–119. [PubMed: 18687410]
6. Xie L, Evangelidis T, Bourne PE. Drug discovery using chemical systems biology: Weak inhibition of multiple kinases may contribute to the anti-cancer effect of nelfinavir. PLOS Comput. Biol. 2011; 7:e1002037. [PubMed: 21552547]
7. Dai W, Jin W, Zhang J, Wang X, Wang J, Zhang X, Wan Y, Zhang Q. Spatiotemporally controlled co-delivery of anti-vasculature agent and cytotoxic drug by octreotide-modified stealth liposomes. Pharm. Res. 2012; 29:2902–2911. [PubMed: 22723122]

8. Sengupta S, Eavarone D, Capila I, Zhao G, Watson N, Kiziltepe T, Sasisekharan R. Temporal targeting of tumour cells and neovasculature with a nanoscale delivery system. Nature. 2005; 436:568–572. [PubMed: 16049491]
9. Szoka F Jr. Papahadjopoulos D. Comparative properties and methods of preparation of lipid vesicles (liposomes). Annu. Rev. Biophys. Bioeng. 1980; 9:467–508. [PubMed: 6994593]
10. Buck E, Eyzaguirre A, Haley JD, Gibson NW, Cagnoni P, Iwata KK. Inactivation of Akt by the epidermal growth factor receptor inhibitor erlotinib is mediated by HER-3 in pancreatic and colorectal tumor cell lines and contributes to erlotinib sensitivity. Mol. Cancer Ther. 2006; 5:2051–2059. [PubMed: 16928826]
11. Smith L, Watson MB, O'Kane SL, Drew PJ, Lind MJ, Cawkwell L. The analysis of doxorubicin resistance in human breast cancer cells using antibody microarrays. Mol. Cancer Ther. 2006; 5:2115–2120. [PubMed: 16928833]
12. Drummond D, Meyer O, Hong K, Kirpotin D, Papahadjopoulos D. Optimizing liposomes for delivery of chemotherapeutic agents to solid tumors. Pharmacol. Rev. 1999; 51:691–743. [PubMed: 10581328]
13. Gabizon A, Horowitz AT, Goren D, Tzemach D, Shmeeda H, Zalipsky S. In vivo fate of folate-targeted polyethylene-glycol liposomes in tumor-bearing mice. Clin. Cancer Res. 2003; 9:6551–6559. [PubMed: 14695160]
14. Gabizon A, Tzemach D, Gorin J, Mak L, Amitay Y, Shmeeda H, Zalipsky S. Improved therapeutic activity of folate-targeted liposomal doxorubicin in folate receptor-expressing tumor models. Cancer Chemother. Pharmacol. 2010; 66:43–52. [PubMed: 19779718]
15. Lee R, Low P. Delivery of liposomes into cultured KB cells via folate receptor-mediated endocytosis. J. Biol. Chem. 1994; 269:3198–3204. [PubMed: 8106354]
16. Lu Y, Low P. Folate-mediated delivery of macromolecular anticancer therapeutic agents. Adv. Drug Deliv. Rev. 2002; 54:675–693. [PubMed: 12204598]
17. Torchilin V. Recent advances with liposomes as pharmaceutical carriers. Nat. Rev. Drug Discov. 2005; 4:145–160. [PubMed: 15688077]
18. Xia W, Low PS. Folate-targeted therapies for cancer. J. Med. Chem. 2010; 53:6811–6824. [PubMed: 20666486]
19. Perche F, Torchilin V. Recent trends in multifunctional liposomal nanocarriers for enhanced tumor targeting. J. Drug Deliv. 2013:705265. 2013. [PubMed: 23533772]
20. Aryal S, Hu CMJ, Zhang L. Polymeric nanoparticles with precise ratiometric control over drug loading for combination therapy. Mol. Pharm. 2011; 8:1401–1407. [PubMed: 21696189]
21. Fang RH, Aryal S, Hu CMJ, Zhang L. Quick synthesis of lipid–polymer hybrid nanoparticles with low polydispersity using a single-step sonication method. Langmuir. 2010; 26:16958–16962. [PubMed: 20961057]
22. Hu CMJ, Aryal S, Zhang L. Nanoparticle-assisted combination therapies for effective cancer treatment. Ther. Deliv. 2010; 1:323–334. [PubMed: 22816135]
23. Singh A, Dilnawaz F, Mewar S, Sharma U, Jagannathan NR, Sahoo SK. Composite polymeric magnetic nanoparticles for co-delivery of hydrophobic and hydrophilic anticancer drugs and MRI imaging for cancer therapy. ACS Appl. Mater. Interfaces. 2011; 3:842–856. [PubMed: 21370886]
24. Wong HL, Bendayan R, Rauth AM, Wu XY. Simultaneous delivery of doxorubicin and GG918 (Elacridar) by new polymer-lipid hybrid nanoparticles (PLN) for enhanced treatment of multidrug-resistant breast cancer. J. Control. Release. 2006; 116:275–284. [PubMed: 17097178]
25. Baeza A, Guisasola E, Ruiz-Hernández E, Vallet-Regí M. Magnetically triggered multi-drug release by hybrid mesoporous silica nanoparticles. Chem. Mater. 2012; 24:517–524.
26. Patel NR, Rathi A, Mongayt D, Torchilin VP. Reversal of multidrug resistance by co-delivery of tariquidar (XR9576) and paclitaxel using long-circulating liposomes. Int. J. Pharm. 2011; 416:296–299. [PubMed: 21703341]
27. Smith RC, Riollano M, Leung A, Hammond PT. Layer-by-layer platform technology for small-molecule delivery. Angew. Chem. Int. Ed. Engl. 2009; 48:8974–8977. [PubMed: 19847838]
28. Janes KA, Reinhardt HC, Yaffe MB. Cytokine-induced signaling networks prioritize dynamic range over signal strength. Cell. 2008; 135:343–354. [PubMed: 18957207]

29. Yokoyama M, Okano T, Sakurai Y, Suwa S, Kataoka K. Introduction of cisplatin into polymeric micelle. J. Control. Release. 1996; 39:351–356.

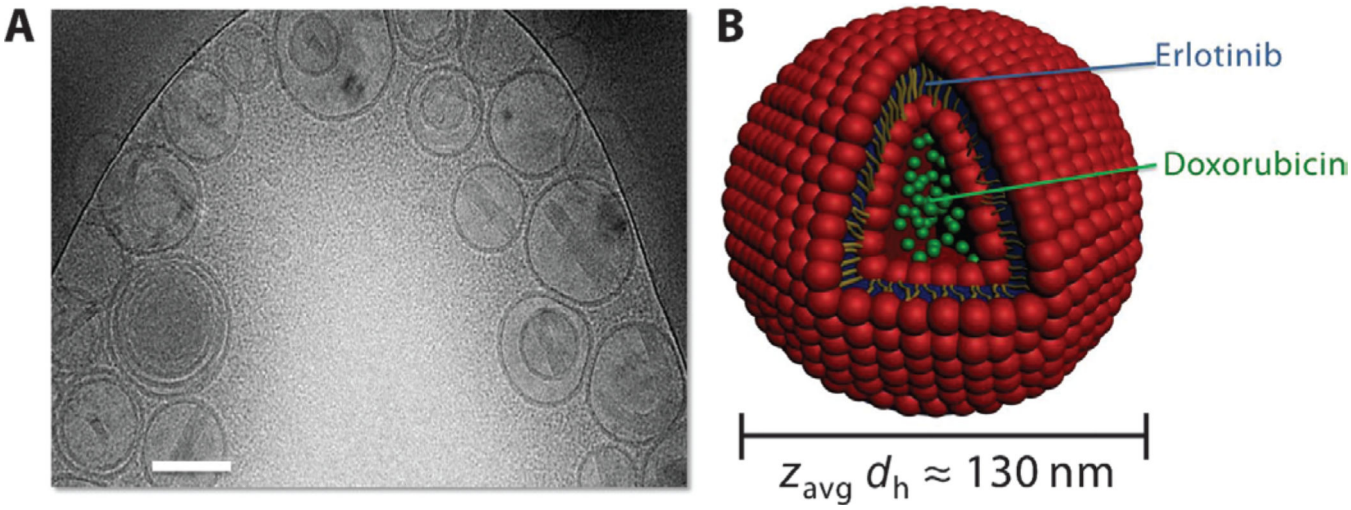

Fig. 1. Characterization of the combination therapeutic–loaded liposomal system

(**A**) Cryogenic transmission electron micrograph of dual drug–loaded liposomes. Scale bar, 100 nm. (**B**) Schematic of dual loading of a small-molecule inhibitor (erlotinib, blue) into the hydrophobic, vesicular wall compartment and of a cytotoxic agent (doxorubicin, green) into the aqueous, hydrophilic interior.

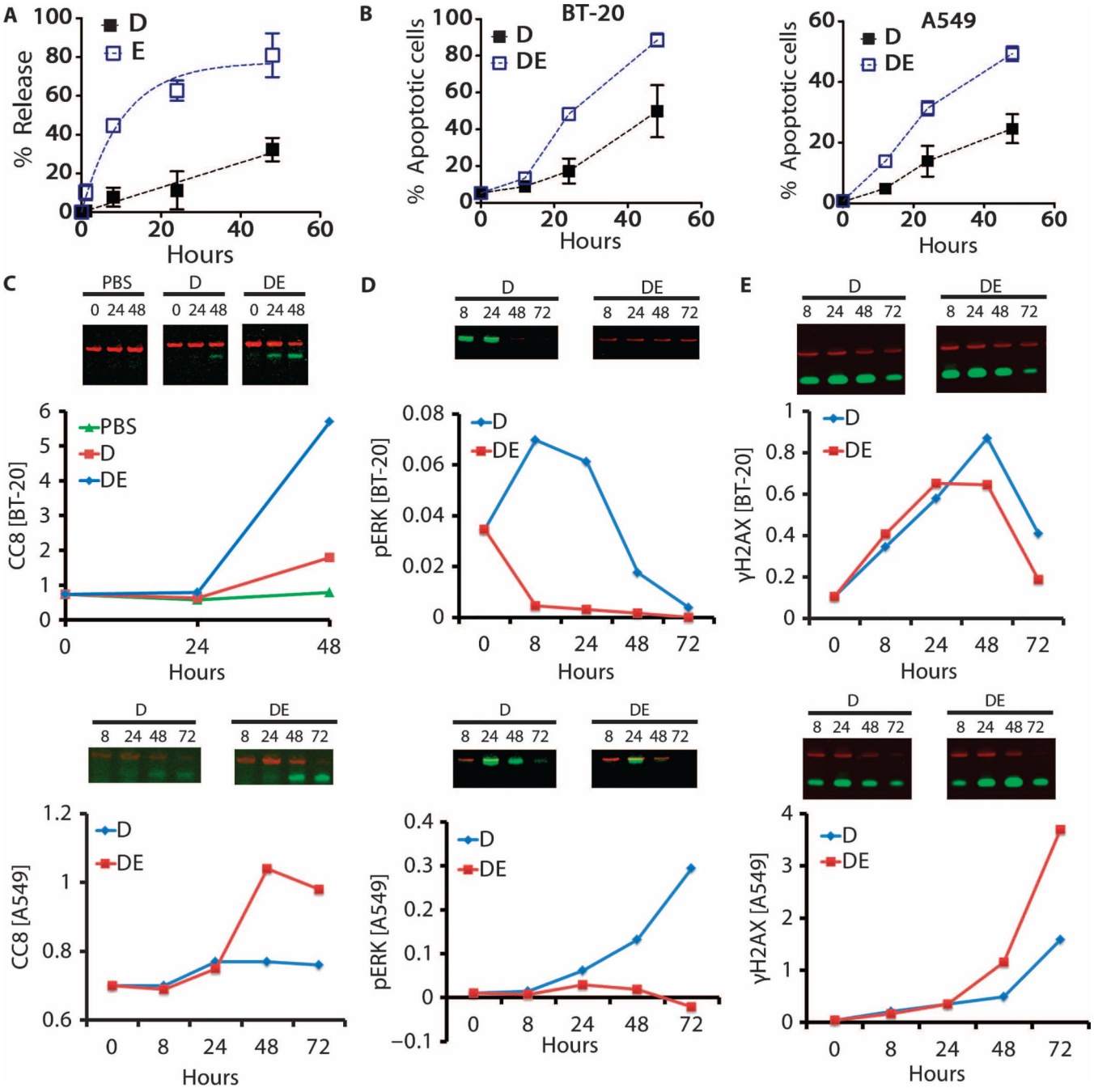

Fig. 2. Evaluation of the dual drug–loaded liposomal system in vitro

(**A**) Drug release from dual drug–loaded liposomes in an excess volume of PBS (pH 7.4) at 37°C under agitation. (**B**) Comparative cytotoxicity of dual drug–loaded liposome relative to the single drug–loaded liposome in BT-20 (TNBC) and A549 (NSCLC) cell lines. This was measured by staining against cleaved caspase-3 and PARP. (**C**) Cleaved caspase-8 in BT-20 cells (top) and A549 cells (bottom) after addition of the indicated liposomes. In the gel images, red is actin and green is cleaved caspase-8. Quantification shown below stained gel images corresponds to relative signal of cleaved caspase-8 to actin. Data are presented as

mean ± SEM of three experiments. (**D**) Dynamics of pERK in BT-20 cells (top) and A549 cells (bottom) after addition of the indicated liposomes. Data are representative of three experiments, and for quantification, pERK abundance was normalized to actin. (**E**) γH2AX formation in BT-20 cells (top) and A549 cells (bottom) after addition of the indicated liposomes. Data are representative of three experiments, and for quantification, γH2AX abundance was normalized to actin. D, doxorubicin only (single drug); DE, doxorubicin and erlotinib (dual drug).

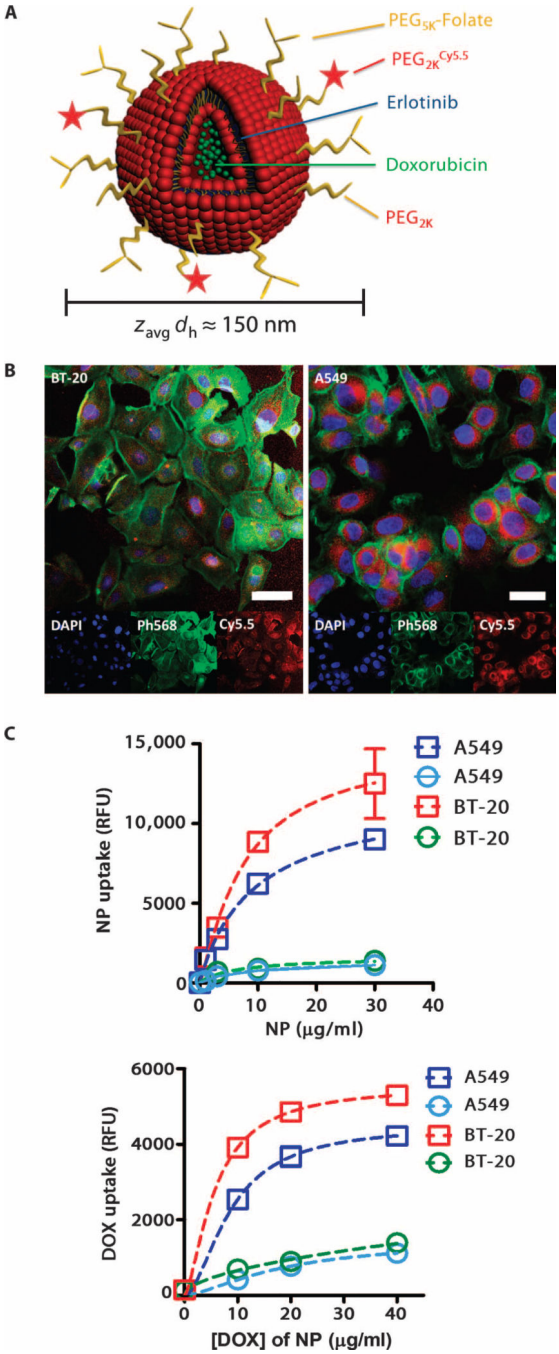

Fig. 3. Decoration of combination therapeutic–loaded liposomes for targeted delivery

(**A**) Schematic of addition of DSPE-PEG_{2K} (0.5 mol % ratio) to minimize nonspecific protein binding, DSPE-$PEG_{2K}^{Cy5.5}$ (0.1 mol % ratio) for fluorescent tracking, and DSPE-PEG_{5K}-folate (0.5 mol % ratio) for cell-targeted delivery. (**B**) Cell uptake of the folate-targeted liposomes in BT-20 and A549 cells, visualized by confocal microscopy. Blue, nuclei labeled with DAPI; green, actin labeled with phalloidin-568 (Ph568); red, DSPE-$PEG_{2K}^{Cy5.5}$–labeled DFP liposomes. Bottom panels represent the fluorescence in each channel; top panels are merged images. (**C**) Cell-associated fluorescence measured by flow

cytometry as a function of nanoparticle (NP) concentration in both cell lines after incubation with liposomes containing or lacking folate at 37°C for 1 hour. Top: Cy5.5 (λ_{ex} = 675 nm, λ_{ex} = 710 nm) corresponding to liposomal association for both targeted (DFP-Cy5.5, squares) and untargeted control (DP-Cy5.5, circles). Bottom: Amount of doxorubicin associated with the cells [doxorubicin fluorescence, (λ_{ex} = 480 nm, λ_{ex} = 560 nm)] for both targeted (DFP-Cy5.5, squares) and untargeted control (DP-Cy5.5, circles). Data are presented as mean ± SEM of three experiments.

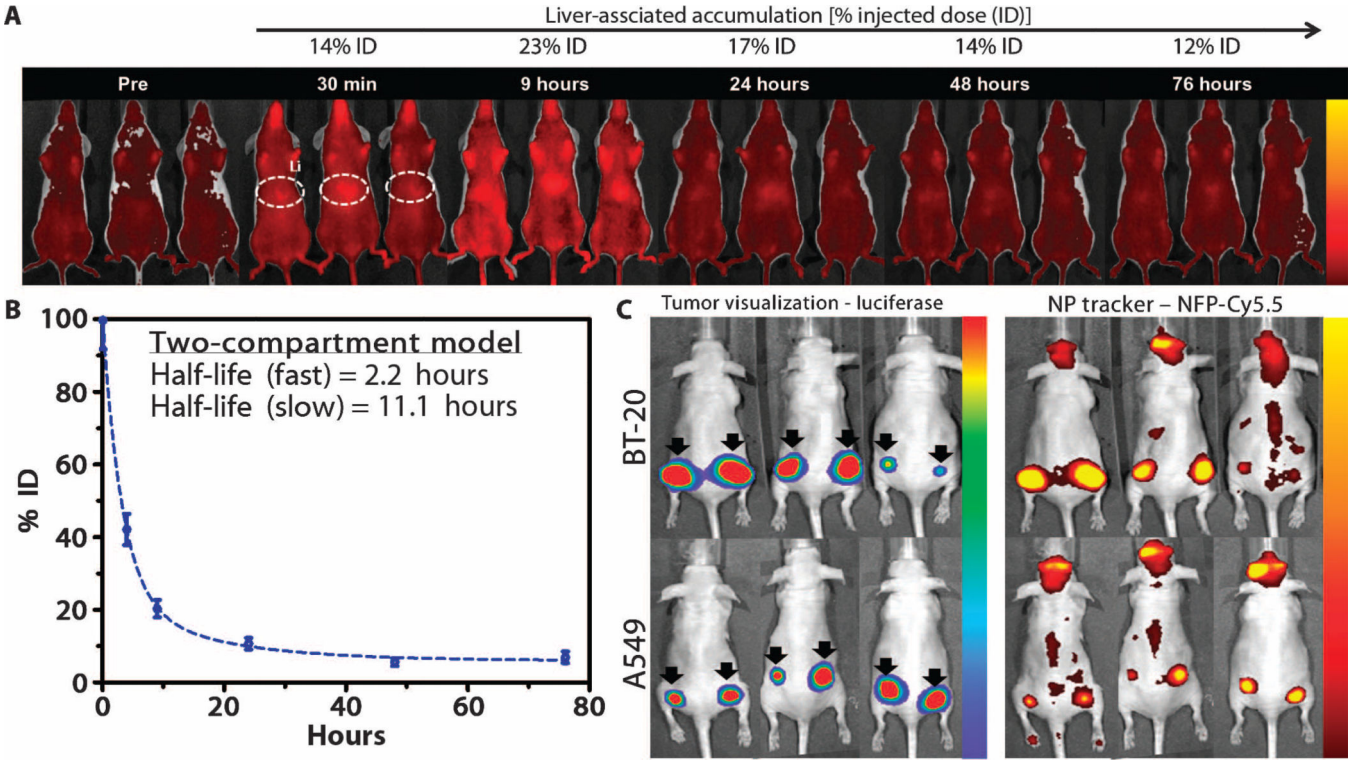

Fig. 4. Biological performance of the folate-targeted liposomal system in vivo

(**A**) Biodistribution panel of folate-targeted liposomes containing no drug (tracked through Cy5.5 fluorescence) that were intravenously administered to BALB/c mice. In situ quantification (region identified with circle at 30 min after injection) of liver-associated nanoparticle fluorescence (normalized to injected dose) presented above each time point. (**B**) Circulation data displayed as percent injected dose (ID), on the basis of nanoparticle Cy5.5 fluorescence recovered in blood samples. Half-life calculated on the basis of a two-compartment model and presented as mean ± SEM. (**C**) Tumor visualization (left; visualized as firefly luciferase expressed in the xenografted cells) and nanoparticle visualization (right; visualized by Cy5.5 fluorescence) 30 days after injection of single 0.1-ml administration of folate-targeted empty liposomes (NFP-Cy5.5) to NCR nude mice bearing BT-20 or A549 xenografts on the hind flanks. The same animals are shown on the left and right images. See fig. S2 for tissue necropsy.

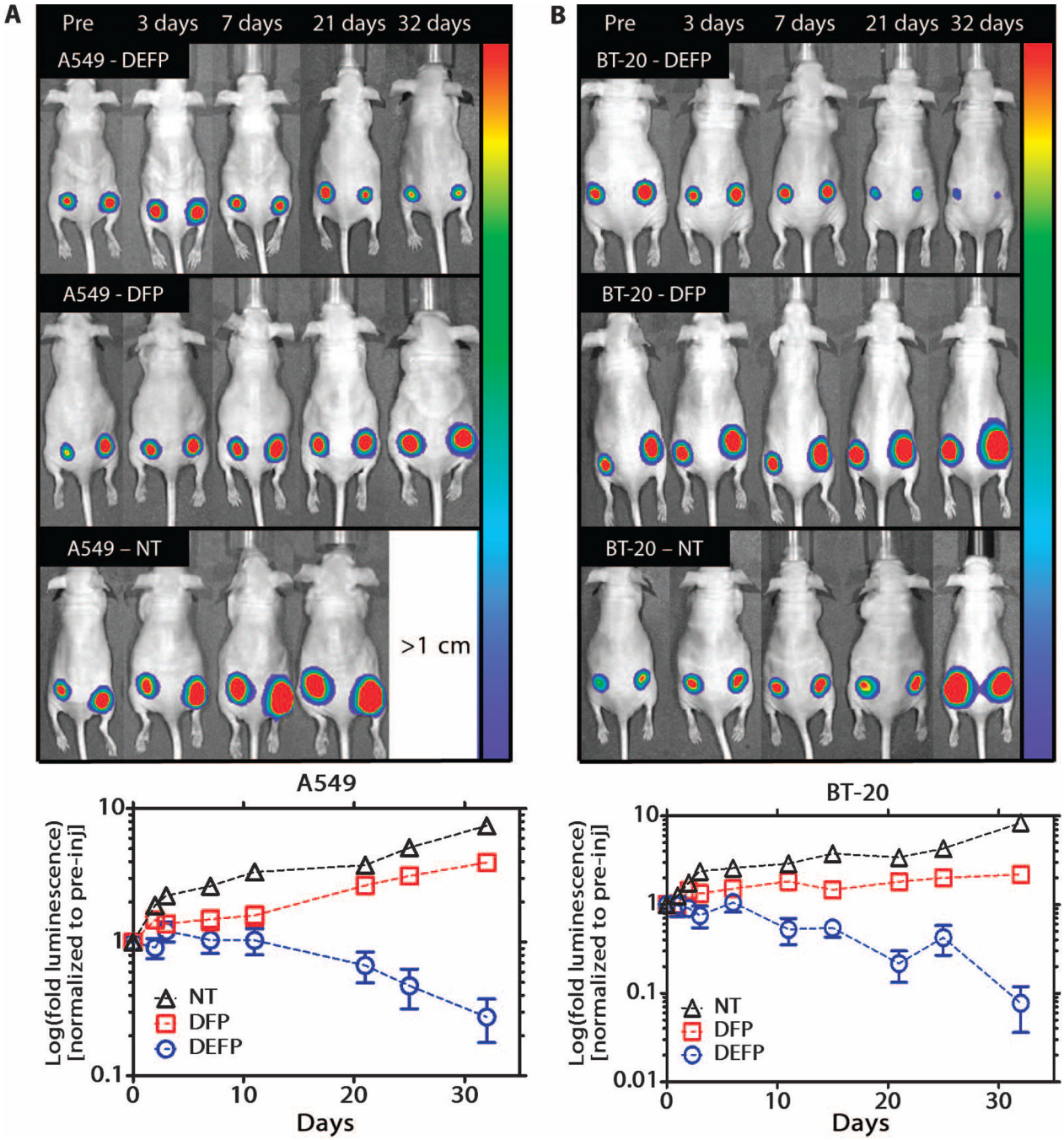

Fig. 5. Effect of dual drug– or single drug–loaded, folate-targeted liposomes on A549 and BT-20 tumor size

(**A**) A549-luciferase–expressing, xenograft-bearing NCR nude mice; n = 5, quantification representative of mean ± SEM (see fig. S5 for all five mice). (**B**) BT-20-luciferase–expressing, xenograft-bearing NCR nude mice; n = 5, quantification representative of mean ± SEM (see fig. S4 for all five mice). Tumor-imaging data for dual drug (DEFP, top), single drug (DFP, middle), and untreated control, along with luminescence quantification (reported as fold initial tumor luminescence, presented on a semi-log plot) corresponding to tumor

size as a function of time, after a single administration of drug (1 mg/kg)–loaded liposomal formulations. Animals with tumor reaching 1 cm were sacrificed. An unpaired, two-tailed t test comparing the DFP and DEFP at the terminal 32-day time point shows statistical significance with P values of 0.0057 and 0.001 for treated A549 and BT-20 xenograft–bearing mice, respectively. A one-way analysis of variance (ANOVA) comparing all treatments for the duration of the experiment (all time points) was also performed for each xenograft cell line, and P values of 0.0024 and 0.0010 were obtained for A549 and BT-20 cells, respectively.

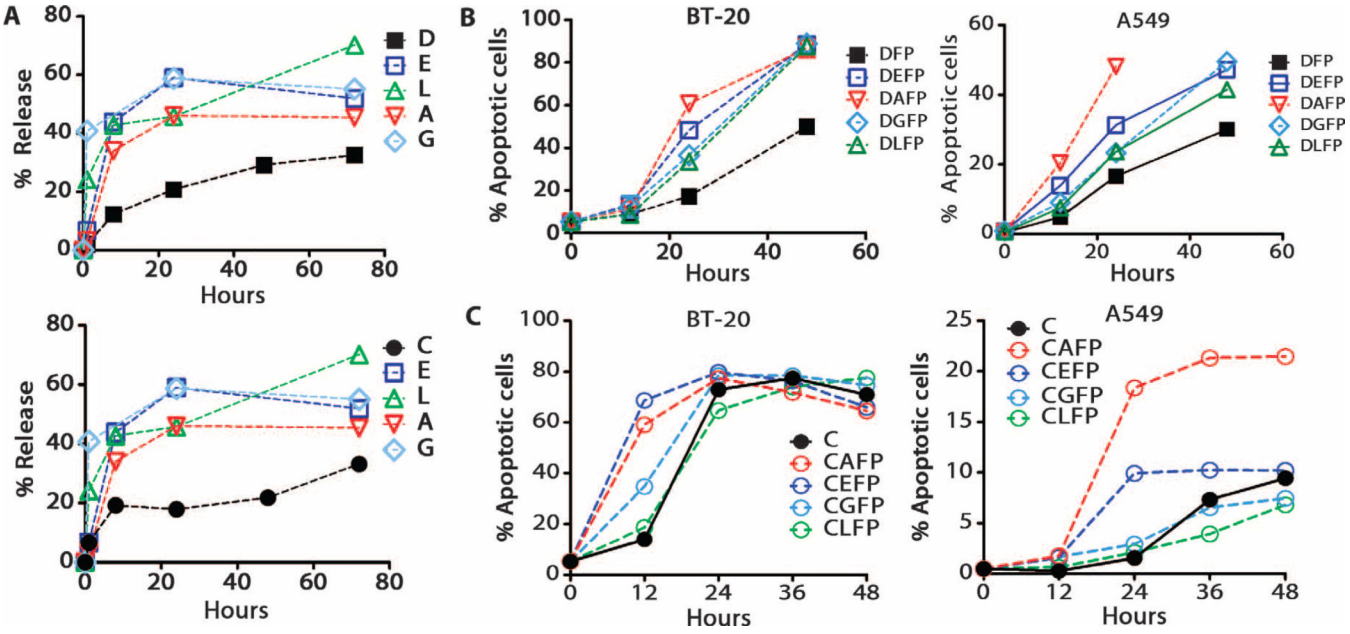

Fig. 6. Developing the RTK inhibitor–cytotoxic agent combination liposomal system as a platform for dual-drug delivery

(**A**) In vitro drug release from dual drug–loaded folate-targeted liposomal formulations. Top: Release from folate and PEG–containing liposomes (FP) with doxorubicin and the indicated RTK inhibitor. Bottom: Release from folate and PEG–containing liposomes (FP) with cisplatin and the indicated RTK inhibitor. Liposomes were incubated with PBS (pH 7.4) at 37°C under agitation in sink conditions. Data are presented as mean of triplicate experiments. (**B**) Cytotoxicity of dual drug–loaded (RTK and doxorubicin) liposomes compared with that of single drug–loaded (doxorubicin) liposomes against BT-20 and A549 cells. Data are presented as mean of triplicate experiments. (**C**) Cytotoxicity of dual drug–loaded (RTK and cisplatin) liposomes compared with that of single drug–loaded (cisplatin) liposomes against BT-20 and A549 cells. Data are presented as mean of triplicate experiments. D, doxorubi-cin; A, afatinib; E, erlotinib; G, gefitinib; L, lapatinib; C, cisplatin; F, folate; P, PEG.

Table 1

Dynamic light scattering, PDI, and potential measurements for the dual-drug and single-drug uncoated and coated (FP) liposomal systems, as measured in 10 mM NaCl at 25°C.

Liposomal formulation	Mean $z_{avg}d_h$ (nm) ± SEM	PDI	ζ potential (mV)	Encapsulation efficiency (%)	w/w % (drug/lipid)
DE	136 ± 10	0.13	−29	D: 97	D: 5.4
				E: 40	E: 2.2
D	126 ± 16	0.15	−27	D: 97	D: 5.5
DFP	156 ± 7	0.1	−17	D: 97	D: 5.4
DEFP	151 ± 14	0.16	−15	D: 97	D: 5.5
				E: 40	E: 2.2

Encapsulation efficiency (% loaded from amount supplied) and mass loading ratio (g/g, drug/lipid) as determined by high-performance liquid chromatography (HPLC). DE, doxorubicin and erlotinib; D, doxorubicin; DFP, doxorubicin, folate, PEG; DEFP, doxorubicin and erlotinib, folate, PEG.

Sci Signal. Author manuscript; available in PMC 2014 November 13.

Table 2

Propertiesofliposomes containing doxorubicin.

Liposomal formulation	Mean $z_{avg}d_h$ (nm) ± SEM	PDI	Encapsulation efficiency (%)	w/w % (drug/lipid)
DFP	156 ± 7	0.1	D: 97	D: 5.4
DAFP	174 ± 13	0.19	D: 99	D: 5.5
			A: 82	A: 4.4
DEFP	151 ±14	0.16	D: 97	D: 5.5
			E: 40	E: 2.2
DGFP	160 ±11	0.12	D: 98	D: 5.5
			G: 85	G: 4.6
DLFP	182 ± 9	0.13	D: 97	D: 5.5
			L: 70	L: 3.8

Dynamic light scattering and PDI measurements conducted in 10 mM NaCl at 25°C for the various dual-drug and single-drug liposomal formulations containing doxorubicin. Encapsulation efficiency (% loaded from amount supplied) and mass loading ratio (g/g drug/lipid) as determined by HPLC. D, doxorubicin; A, afatinib; E, erlotinib; G, gefitinib; L, lapatinib; C, cisplatin; F, folate; P, PEG. Corresponding formulations without folate-PEG (FP) are shown in table S1.

Table 3

Properties of liposomes containing cisplatin.

Liposomal formulation	Mean $z_{avg}d_h$ (nm) ± SEM	PDI	Encapsulation efficiency (%)	w/w % (drug/lipid)
CFP	183 ± 12	0.16	C: 62	C: 11
CAFP	177 ± 6	0.06	C: 58	C: 9.9
			A: 73	A: 5.2
CEFP	183 ± 13	0.16	C: 60	C: 10.5
			E: 34	E: 2.4
CGFP	162 ± 8	0.09	C: 55	C: 9.4
			G: 81	G: 5.8
CLFP	204 ±11	0.11	C: 60	C: 10.2
			L: 72	L: 5.1

Dynamic light scattering, PDI, and ζ potential measurements conducted in 10 mM NaCl at 25°C for the various multidrug liposomal formulations containing cisplatin. Encapsulation efficiency (% loaded from amount supplied) and mass loading ratio (g/g drug/lipid) as determined by HPLC. D, doxorubicin; A, afatinib; E, erlotinib; G, gefitinib; L, lapatinib; C, cisplatin; F, folate; P, PEG. Corresponding formulations without folate-PEG (FP) are shown in table S1.